*Desalination and Water Treatment*
www.deswater.com

doi: 10.5004/dwt.2023.29294

284 (2023) 175–181
February

# Remediation of $PO_4^{3-}$ and $Ni^{2+}$ from aqueous solution by novel jarosite: competitive adsorption performance and mechanism

Rui Han[a], Shengtao Wang[a], Yilin Xu[b], Zhenxing Wang[a,*], Haoquan Yu[a], Fan Yang[a]

[a]*The Development Construction Co., Ltd., of China Construction Eighth Engineering Division, Qingdao 266061, China, Tel.: +86 15253285729; emails: dzwangzhenxing@163.com (Z. Wang), hrhyj@126.com (R. Han), yxcp@163.com (S. Wang), yhqyhqyhq163@163.com (H. Yu), 18660279553@163.com (F. Yang)*
[b]*State Key Laboratory of Pollution Control and Resources Reuse, College of Environmental Science and Engineering, Tongji University, Shanghai 200092, China, email: 15227585680@163.com*

Received 2 July 2022; Accepted 25 December 2022

**ABSTRACT**

The wastewater containing both $PO_4^{3-}$ and $Ni^{2+}$ (e.g., nickel plating) causes a strong threat on the environment and human health. In this study, novel jarosite was prepared by using the chemical oxidation method as natural adsorbent and was employed for simultaneous $PO_4^{3-}$ and $Ni^{2+}$ removal in aqueous solution. The results revealed that as-synthesized jarosite had sea urchin-like morphology with the 2–4 nm needle burr structure and developed $S_{BET}$ (215.6 $m^2/g$) and pore structure. The adsorption capacity of $Ni^{2+}$ on jarosite increases significantly as the concentration of $PO_4^{3-}$ increases, and when the concentration of phosphoric acid increases, the maximum adsorption capacity of $Ni^{2+}$ on jarosite (0.22 mmol/g) under 4.0 mM $PO_4^{3-}$ is approximately 1.6 times than that of pure $Ni^{2+}$ solution (0.14 mmol/g), indicating that the presence of $PO_4^{3-}$ reduces the electrostatic repulsion between jarosite and $Ni^{2+}$. pH can significantly affect the adsorption of $PO_4^{3-}$ and $Ni^{2+}$ on jarosite by electrostatic interaction. The proposed adsorption mechanism for $PO_4^{3-}$ and $Ni^{2+}$ includes porous entrapment, ion exchange, electrostatic attraction and surface mineral precipitation/complexation.

*Keywords:* Jarosite; $PO_4^{3-}$; $Ni^{2+}$; Competitive adsorption; Adsorption mechanism

## 1. Introduction

The increasingly developed industrial and agricultural production has not only brought a more convenient life to human beings, but also led to worldwide environmental pollution, among which water pollution has become a major concern [1]. Phosphate ($PO_4^{3-}$) and $Ni^{2+}$ are both typical pollutants in the water environment, $Ni^{2+}$ has been considered the most critical environmental pollutants due to their carcinogenic nature and longer persistent in the environment [2–4]. Excessive $Ni^{2+}$ is toxic to blood and kidneys cells and causes skin diseases, allergies, or cancer. Moreover, excess $PO_4^{3-}$ in water can lead to eutrophication of water bodies and impair the quality of the aquatic environment, as well as play a crucial role in gene synthesis and energy transfer in biological systems.

As a result, the focus of research on wastewater remediation shifts to the development of efficient methods for removing $PO_4^{3-}$ and $Ni^{2+}$. Up to now, adsorption technology is considered one of the most environment friendly and highly efficient options [5]. Activated carbon and molecular sieves were widely used because of their distinctive adsorption properties, resulting from firm micro and mesoporous structures [6,7]. However, their high cost, complex preparation and recycling methods remain a major obstacle to the large-scale application [8].

Natural jarosite [$KFe_3(SO_4)_2(OH)_6$] is a kind of hydrated iron oxide rich in sulfate, with weak crystallinity and a

* Corresponding author.

large specific surface area [9,10]. Acidic mine wastewater (AMD), acid sulfate soil, and their environs are frequently discovered to include natural jarosite, which regulates and influences the form, migration, and return of various heavy metal contaminants and oxygen-containing anions in this environment [11,12]. Moreover, the higher oxygen content and acidic groups of jarosite also play a part in increasing its $PO_4^{3-}$ and $Ni^{2+}$ adsorption efficiency [13,14]. In addition, jarosite has the advantages of wide range, easy access and low toxicity. Therefore, jarosite was expected to become an efficient adsorption material for water treatment.

The preparation of jarosite and examination of its effectiveness in eliminating $PO_4^{3-}$ and $Ni^{2+}$ from aqueous solution were the two main objectives of this investigation. To address this aim, our study mainly includes: (1) preparing and characterizing jarosite; (2) determining the effects of pH, contact time and initial pollutant concentration on competitive adsorption efficiency; (3) further study on competitive adsorption mechanisms of the pollutant.

## 2. Materials and methods

### 2.1. Materials

NaOH, $HNO_3$, $FeSO_4{\cdot}7H_2O$, $K_2SO_4$, $NaH_2PO_4$, $Ni(NO_3)_2$ in this work were obtained from Sinopharm Chemical Reagent Co., Ltd., (China) at analytical grade and used without further purification (China). The standard $PO_4^{3-}$ and $Ni^{2+}$ stock solution of 10 mmol/L were prepared by dissolving the specific quality pollutants ($NaH_2PO_4$, $Ni(NO_3)_2$) in deionized water (18.0 MΩ cm). Deionized water was produced from a Millipore Milli-Q Ultrapure Gradient A10 purification system. Experimental solutions of desired concentration were configured by diluting the stock solution with deionized water.

### 2.2. Preparation method

The preparation method of jarosite refer to the previous work with slight modifications [15]. As shown in Fig. 1, the 13.90 g $FeSO_4{\cdot}7H_2O$ and 1.48 g $K_2SO_4$ was impregnated in deionized water under magnetic stirring (500 rpm) at 85°C for 60 min. The obtained samples were subsequently soaked with deionized water and rinsed with deionized water to neutral (pH = 7). Finally, the samples were dried at 85°C for 6 h, and then allowed to cool to room temperature. The ultimately acquired samples were denoted as jarosite.

### 2.3. Characterization of as-synthesized jarosite

The surface morphology of as-synthesized were observed by scanning electron microscopy (SEM, Zeiss Supra 40, Germany) and microstructures were identified by high-resolution transmission electron microscopy (HRTEM, Zeiss Libra 200). The textural parameters including specific surface area, total pore volume, and $N_2$ adsorption/desorption isotherms were determined by Brunauer–Emmett–Teller (BET) (GEMINI VII 2390, USA). The crystal phase structure of as-synthesized were presented by X-ray diffraction (XRD, D/max-1200X, Cu K$\alpha$ radiation ($\lambda$ = 1.5406 Å) operating. Point of zero charge (PZC) was used to determine the surface charges of jarosite [16].

### 2.4. Adsorption experiments

#### 2.4.1. Solution configuration and measurement

The concentration of $PO_4^{3-}$ was determined by the ammonium molybdate spectrophotometric method. The concentration of $Ni^{2+}$ was determined by ICP-OES analyzer (iCAP6300, Thermo, USA) [17]. The adsorption capacity $Q_e$ (mmol/L) and removal rate (%) of jarosite were calculated by:

$$Q_e = \frac{(C_0 - C_e)V}{M} \tag{1}$$

$$\text{Removal}(\%) = \frac{(C_0 - C_e)}{C_0} \times 100\% \tag{2}$$

where $C_o$ and $C_e$ are the initial and equilibrium concentrations of the $PO_4^{3-}$ and $Ni^{2+}$ (mmol/L), respectively, $V$ is the volume (L), and $M$ is the mass of carbons used (g). Three-sample t-tests were used to evaluate the significant difference of each group. The data were all the average of two or more replicates. When the p-value was less than 0.05, the results were deemed statistically significant.

#### 2.4.2. Adsorption kinetics

The kinetic experiments were done to investigate the effect of contact time and evaluate the kinetic properties. The pollutant solutions with specific concentration ($PO_4^{3-}$ (0.5 mM) alone or $Ni^{2+}$ (0.2 mM) alone) were configured in a 2 L beaker and stirred with a magnetic stirrer (300 rpm) at

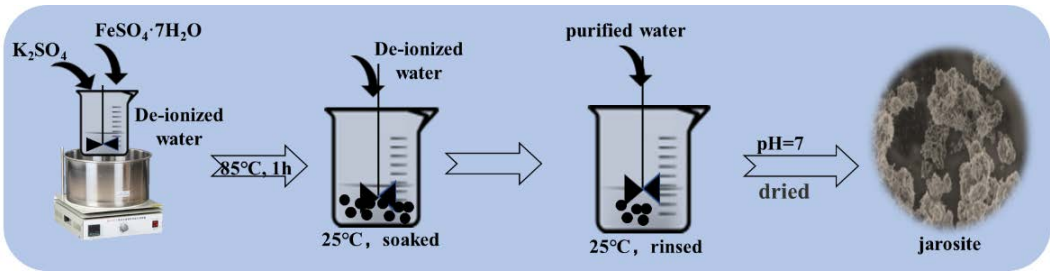


Fig. 1. Fabrication of jarosite.

25°C ± 1°C. The mixture solution had specific initial pH (5.0) by NaOH and $HNO_3$, which was detected using a pH meter (Model PHS-3C, Shanghai, China). The kinetic reactions were initiated by spiking as-synthesized jarosite (0.20 g) into the pollutant solutions. Then 5 mL of solution samples were taken at a desired time interval within the set time range (0–48 h). The solution sample was filtered through a 0.45 μm membrane, and the residual concentration of pollutants was detected using the method mentioned in 2.4.1.

*2.4.3. Competitive adsorption and adsorption isotherms*

Batch competitive adsorption experiments were carried out by 0.01 g as synthesized jarosite into brown conical flasks (250 mL) containing pollutant solution (100 mL) with $PO_4^{3-}$ solution (0.5–2.5 mM) to investigate the effects of $Ni^{2+}$ ionic strength (1 and 2 mM) on the adsorption. At the same time, batch competitive adsorption experiments were carried out by 0.01 g as-synthesized jarosite into brown conical flasks (250 mL) containing pollutant solution (100 mL) with $Ni^{2+}$ solution (0.1–1 mM) to investigate the effects of $PO_4^{3-}$ ionic strength (1.5 and 3 mM) on the adsorption. The conical flask was then shaken at 200 ± 10 rpm in a shaded water bath shaker (SHZ-88) at 25°C ± 1°C for 24 h until the equilibrium was achieved. Finally, the concentration of the remaining pollutant solution was determined.

*2.4.4. Effect of initial pH*

To explore the adsorption performance of pollutants on as-synthesized jarosite at different initial pH values, a certain amount of as-synthesized jarosite was added into a conical flask (150 mL) containing 50 mL of the pollutant solution $PO_4^{3-}$ (1.6 mM) and $Ni^{2+}$ (0.2 mM) with different initial pH values (pH = 3–7).

*2.4.5. Analysis methods*

Statistical analysis uses the SPSS statistical software package (SPSS 23.0, IBM Corp., New York, USA). Graphs were plotted using the Origin 9.0 software.

## 3. Results and discussion

### *3.1. Textural characteristics of jarosite*

Based on the SEM and transmission electron microscopy (TEM) observations and analysis of as-synthesized jarosite, the sea urchin-like morphology [18] with the 2–4 nm needle burr structure [19] was observed in Fig. 2a and b. The surfaces of as-synthesized jarosite were rough, and pores of different sizes and irregular structures had been developed, which is conducive to improve their adsorption characteristics [20]. The XRD patterns of the as-synthesized jarosite

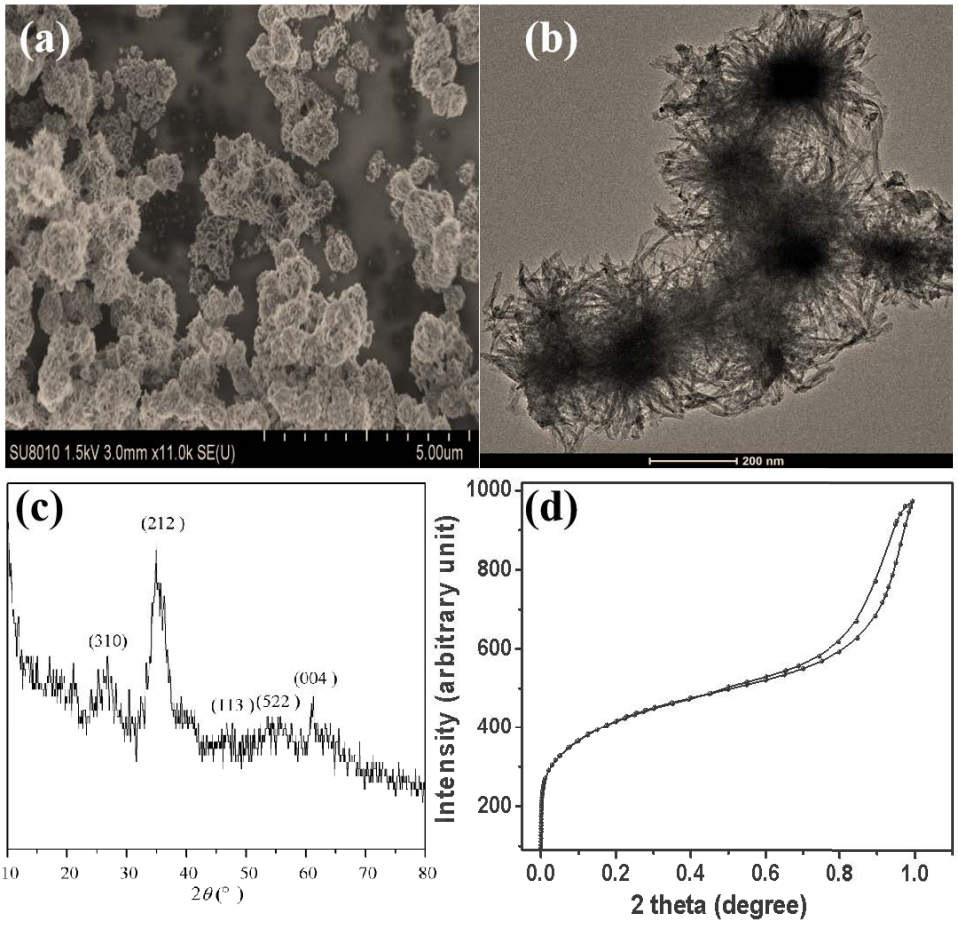


Fig. 2. SEM (a) and TEM (b); XRD spectrum (c) and $N_2$ adsorption/desorption isotherms (d) of as-synthesized jarosite.

are shown in Fig. 2c. The peaks at 2θ values 24.36°, 35.2°, 49.98°, and 62.54° in as-synthesized jarosite were observed, which could be assigned to the planes of the jarosite structure (PDF 29-0713) [21]. The results suggested that the prepared materials was jarosite. The $S_{BET}$ of as-synthesized jarosite was 215.6 $m^2/g$ accordance to the result of the $N_2$ adsorption/desorption isotherms were determined by Brunauer–Emmett–Teller (BET), the big BET could improve physical adsorption properties of jarosite. As shown in Fig. 2d, condensation and hysteresis of isotherms (in higher $P/P_0$) showed that the isotherm is of I and IV hybrid with well-defined H3-type hysteresis loop according to the IUPAC [22], which was characteristic for mesoporous materials.

### 3.2. Adsorption kinetics

As shown in Fig. 3a, the adsorption capacity of $PO_4^{3-}$ and $Ni^{2+}$ on as-synthesized jarosite increased with the contact times. The adsorption capacity of $PO_4^{3-}$ and $Ni^{2+}$ increased rapidly in the initial stage of reaction (1–2 h), then the increase became slow and finally reached a dynamic equilibrium due to initial as-synthesized jarosite's enough adsorption sites for $PO_4^{3-}$ and $Ni^{2+}$ adsorption. With the increase of time, the number of adsorption sites on the surface of applied minerals decreases, and $Ni^{2+}$ and $PO_4^{3-}$ need more time to be adsorbed on the surface of applied minerals, so the increasing trend of adsorption capacity becomes slow. As the adsorption sites tend to be saturated, the adsorption capacity gradually tends to be stable [23,24].

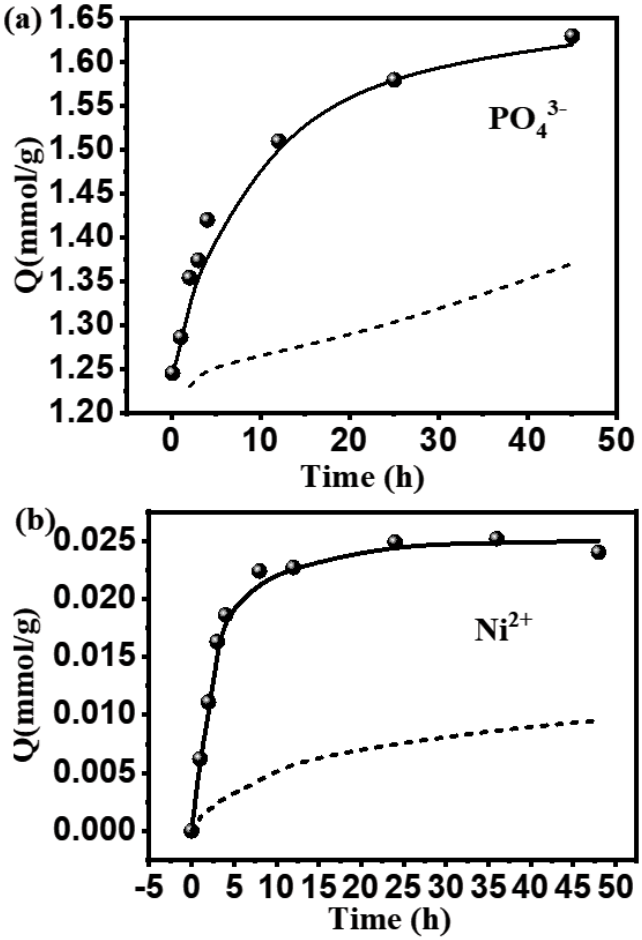


Fig. 3. Adsorption kinetics fitted by pseudo-first-order (solid lines) and pseudo-second-order models (solid lines) for $PO_4^{3-}$ (a) and $Ni^{2+}$ (b).

Adsorption processes were analyzed by pseudo-first-order [25] and pseudo-second-order [26] kinetic models. The comparisons of different kinetic models for the adsorption of jarosite are plotted in FFigs. 3a and b. As shown in Table 1, the pseudo-second-order model fit the experimental data quite well with all $R^2$ higher than 0.996, and there were good agreements between $Q_{cal}$ and $Q_{exp}$, so the adsorption of $PO_4^{3-}$ and $Ni^{2+}$ by jarosite obeys the pseudo-second-order model indicating that chemical adsorption is the main adsorption process [27].

### 3.3. Adsorption isotherms and competitive adsorption

The Langmuir isotherm model assumed monolayer coverage of the adsorbate over a homogenous adsorbent surface [28]. By contrast, Freundlich isotherm explains the reversible multi-layer adsorption on adsorbent surfaces. [29] In this study, the adsorption isotherm was thoroughly described using the Langmuir and Freundlich isotherms (Fig. 4). The isotherm models were given by Eqs. (3) and (4):

$$Q_e = \frac{Q_0 K_L C_e}{1 + K_L C_e} \tag{3}$$

$$\ln Q_e = \ln K_F + \frac{1}{n} \ln C_e \tag{4}$$

where $Q_e$ (mmol/g) is the maximum adsorption capacity of adsorbents; $C_e$ (mg/L) is the equilibrium BbFA concentration; $Q_o$ (mmol/g) is the initial adsorption capacity; $K_L$ (L/mg) and

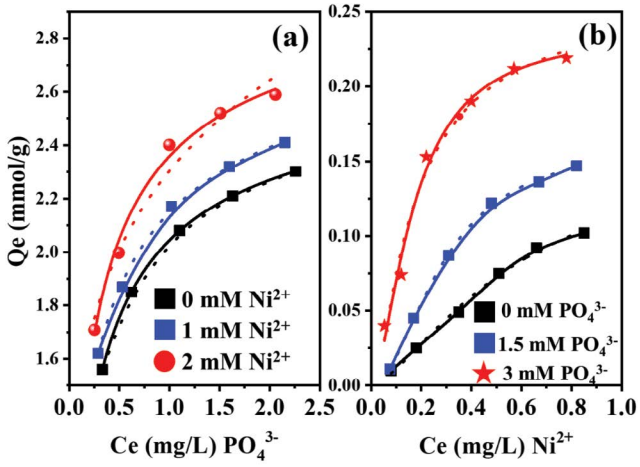


Fig. 4. (a) Adsorption isotherms of $PO_4^{3-}$ on the as-synthesized jarosite at different $Ni^{2+}$ ionic strength and (b) adsorption isotherms of $Ni^{2+}$ on the as-synthesized jarosite at different $PO_4^{3-}$ ionic strength. Solid lines represent the Langmuir isotherms, dash lines represent the Freundlich isotherms.

Table 1
Langmuir and Freundlich isotherms for $PO_4^{3-}$ and $Ni^{2+}$ adsorption

| Model | Parameters | | | |
|---|---|---|---|---|
| $PO_4^{3-}$ | | $[Ni^{2+}]$ = 2 mM | $[Ni^{2+}]$ = 1 mM | $[Ni^{2+}]$ = 0 mM |
| Langmuir | $Q_m$ (mmol/g) | 2.667 | 2.432 | 2.321 |
| | $K_L$ (L/mg) | 0.275 | 0.303 | 0.411 |
| | $R^2$ | 0.983 | 0.999 | 0.997 |
| Freundlich | $K_F$ ((mmol/g)/(L/mg)$^{1/n}$) | 0.271 | 0.155 | 0.115 |
| | n | 0.50585 | 0.244 | 0.578 |
| | $R^2$ | 0.960 | 0.967 | 0.965 |
| $Ni^{2+}$ | | $[PO_4^{3-}]$ = 3 mM | $[PO_4^{3-}]$ = 1.5 mM | $[PO_4^{3-}]$ = 0 mM |
| Langmuir | $Q_m$ (mmol/g) | 0.227 | 0.123 | 0.103 |
| | $K_L$ (L/mg) | 0.163 | 0.238 | 0.166 |
| | $R^2$ | 0.993 | 0.981 | 0.998 |
| Freundlich | $K_F$ ((mmol/g)/(L/mg)$^{1/n}$) | 2.358 | 2.147 | 2.043 |
| | $n$ | 0.169 | 0.178 | 0.265 |
| | $R^2$ | 0.922 | 0.897 | 0.909 |

$K_F$ ((mg/g)/(L/mg)$^{1/n}$) are the Langmuir isotherm constant and Freundlich affinity coefficient, respectively; $n$ is the adsorption intensity.

Table 1 provides a summary of the isotherm lines, constants, and correlation coefficients of isotherm models. From Fig. 4a and Table 1, it is easy to find that the Freundlich model had a better fit to the $PO_4^{3-}$ adsorption process of the jarosite, which indicated that the $PO_4^{3-}$ adsorption tended to be homogeneous and showed monolayer coverage due to the strong interactions between the surface of jarosite and $PO_4^{3-}$. The Langmuir isotherm model also provided the best explanation for the complicated chemical and multi-layer adsorption process that resulted from the hybridization of metal oxides in jarosite during the $Ni^{2+}$ adsorption process onto the material. In addition, the Freundlich constant $n$ values were in the range of 0–1, suggesting that the jarosite composites can actively adsorb $PO_4^{3-}$ and $Ni^{2+}$. Overall, the adsorption of $Ni^{2+}$ and $PO_4^{3-}$ on as-produced jarosite is synergistic.

The results of competitive adsorption can explain the adsorption mechanism for adsorption of $PO_4^{3-}$ and $Ni^{2+}$ on jarosite [30]. The effect of $Ni^{2+}$ on the adsorption of $PO_4^{3-}$ on jarosite is shown in Fig. 4a, the jarosite can effectively adsorb $PO_4^{3-}$ in the absence of $Ni^{2+}$ due to electrostatic attraction. With the increase of $Ni^{2+}$ concentration in $PO_4^{3-}$ solution, the adsorption capacity of phosphoric on jarosite increased, surface mineral precipitation and complexation between $PO_4^{3-}$, $Ni^{2+}$ and jarosite can explain the result. Interestingly, phosphoric can also promote the adsorption of $Ni^{2+}$ onto jarosite in Fig. 4b. According to the effective results of $PO_4^{3-}$ on the adsorption of $Ni^{2+}$ on jarosite, the adsorption of $Ni^{2+}$ is poor in the absence of $PO_4^{3-}$ due to electrostatic repulsion. The adsorption capacity of $Ni^{2+}$ on jarosite increases significantly as the concentration of $PO_4^{3-}$ increases, and when the concentration of phosphoric acid increases, the maximum adsorption capacity of $Ni^{2+}$ on jarosite (0.22 mmol/g) under 4.0 mM $PO_4^{3-}$ is approximately 1.6 times than that of pure $Ni^{2+}$ solution (0.14 mmol/g), indicating that the presence of $PO_4^{3-}$ reduces the electrostatic repulsion between jarosite and $Ni^{2+}$.

### 3.4. Effect of pH on $PO_4^{3-}$ and $Ni^{2+}$ adsorption

As we know, pH is one of the most important significant factors affecting the adsorption process since it influences the degree of ionization and the kind of pollutants already present in addition to the adsorbent surface charge, functions, and adsorption site. For $PO_4^{3-}$ adsorption in Fig. 5a, the removal efficiency of $PO_4^{3-}$ by jarosite decreased with the increasing pH value. According to Fig. 5b, jarosite has an isoelectric point of 7.5. The surface of jarosite is positively charged when pH < 7.5. Because $PO_4^{3-}$ was negatively charged in this instance and was attracted to the surface of jarosite, its removal rate was comparatively high. The adsorption of $PO_4^{3-}$ is likewise lessened as the positive charge on the jarosite surface decreases (pH > 7.0). Depending on the pH value, $Ni^{2+}$ can potentially exist as the species of $Ni^{2+}$ (pH < 8), $Ni(OH)^+$, $Ni(OH)_2^0$, $Ni(OH)_3^-$ and $Ni(OH)_4^{2-}$ [31]. As shown in Fig. 5c, the pH value increased the effectiveness of $Ni^{2+}$ removal by jarosite. This is due to the weak repulsion of positively charged $Ni^{2+}$ due to the decrease of positive charge indicated by as-synthesized jarosite, which is favourable to $Ni^{2+}$ adsorption and the mild repulsion of positively charged $Ni^{2+}$ [32].

### 3.5. Mechanisms of $PO_4^{3-}$ and $Ni^{2+}$ adsorption onto jarosite

Jarosite may hold more $PO_4^{3-}$ and $Ni^{2+}$ ions due to its large specific surface area and well-developed pore structure. Jarosite has a lot of O-containing functional groups (hydroxyl), sulfate and other chemical active groups. Proton release has been suggested to have occurred concurrently with $Ni^{2+}$ adsorption, which was recognized as an ion exchange process [33,34]. The following equation reactions [(5)–(8)] explain this ion-exchange mechanism [4]. Due to electrostatic attraction, jarosite with the positively charged surface can absorb large amounts of metal ions ($Ni^{2+}$) and

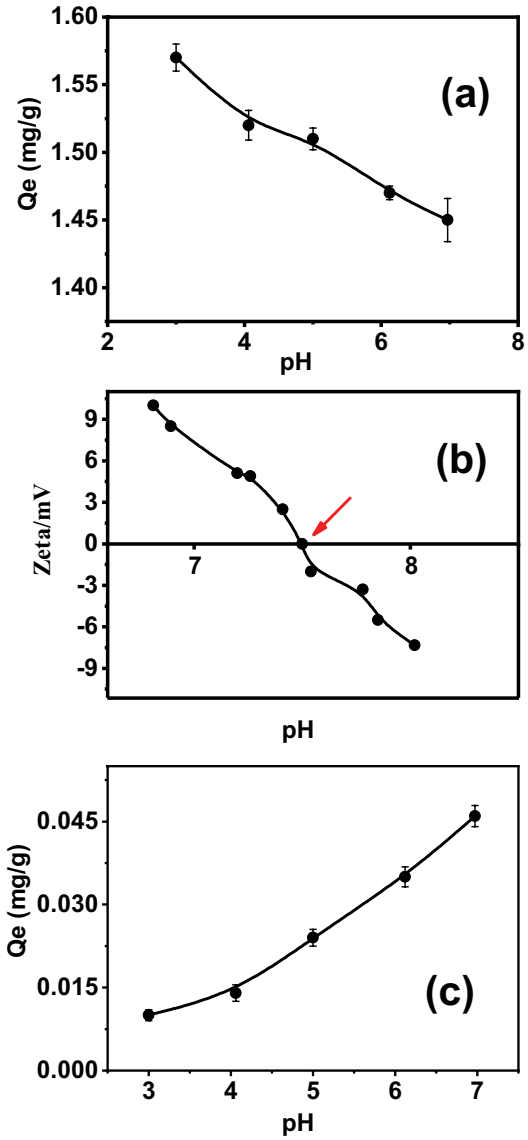


Fig. 5. (a) Effect of initial pH on the removal of $PO_4^{3-}$, (b) the points of zero charge (PZC) onto jarosite and (c) effect of initial pH on the removal of $Ni^{2+}$.

inorganic anions ($PO_4^{3-}$). On the surface of jarosite, $Ni^{2+}$ and $PO_4^{3-}$ can combine to form ternary complexes, which is primarily due to surface complexation and mineral precipitation. Fig. 6 illustrates how the adsorption mechanism was primarily attributed to four processes: surface mineral precipitation and complexation, ion-exchange, electrostatic attraction, and porous entrapment [4].

$$\text{Surface-COOH} + OH^- \leftrightarrow \text{Surface-COO}^- + H_2O \quad (5)$$

$$\text{Surface-OH} + OH^- \leftrightarrow \text{Surface-O}^- + H_2O \quad (6)$$

$$\text{Surface-O}^- + Ni^{2+} \leftrightarrow \text{Surface-O}^- - Ni(II) \quad (7)$$

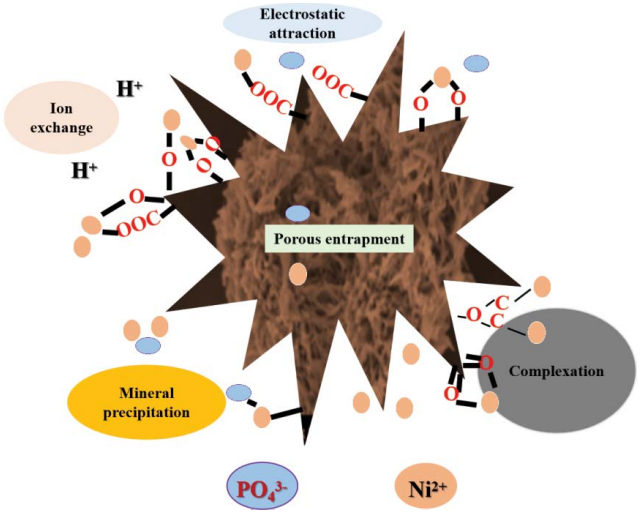


Fig. 6. Schemes of the mechanisms for adsorption of $PO_4^{3-}$ and $Ni^{2+}$ on jarosite.

$$\text{Surface-COO}^- + Ni^{2+} \leftrightarrow \text{Surface-COO}^- - Ni(II) \quad (8)$$

## 4. Conclusions

In this work, the as-prepared jarosite had sea urchin-like morphology and had developed $S_{BET}$ (215.6 $m^2/g$) and pore structure. The isoelectric point of jarosite is 7.5. There is a synergistic adsorption effect between $PO_4^{3-}$ and $Ni^{2+}$ on jarosite, however the effect of $Ni^{2+}$ on $PO_4^{3-}$ adsorption is inferior than that of phosphorus on $Ni^{2+}$ adsorption. pH can significantly affect the adsorption of $PO_4^{3-}$ and $Ni^{2+}$ on jarosite by electrostatic interaction. The proposed adsorption mechanism for $PO_4^{3-}$ and $Ni^{2+}$ includes porous entrapment, ion exchange, electrostatic attraction and surface mineral precipitation/complexation.

## Funding

This research received no external funding.

## Institutional review board statement

Not applicable.

## Informed consent statement

Not applicable.

## Acknowledgment

The authors also gratefully acknowledge the support of those who reviewed this paper and provided many valuable suggestions.

## Conflicts of interest

There are no conflicts of interest.

## References


[1] A.Y. Li, H. Deng, Y.H. Jiang, C.H. Ye, B.G. Yu, X.L. Zhou, A.Y. Ma, Superefficient removal of heavy metals from wastewater by Mg-loaded biochars: adsorption characteristics and removal mechanisms, Langmuir, 36 (2020) 9160–9174.

[2] M.H. Dehghani, M. Sarmadi, M.R. Alipour, D. Sanaei, H. Abdolmaleki, S. Agarwal, V.K. Gupta, Investigating the equilibrium and adsorption kinetics for the removal of Ni(II) ions from aqueous solutions using adsorbents prepared from the modified waste newspapers: a low-cost and available adsorbent, Microchem. J., 146 (2019) 1043–1053.

[3] A. Ma, A. Abushaikha, S.J. Allen, G. McKay, Ion exchange homogeneous surface diffusion modelling by binary site resin for the removal of nickel ions from wastewater in fixed beds, Chem. Eng. J., 358 (2019) 1–10.

[4] W. Yin, C. Zhao, J. Xu, J. Zhang, Z. Guo, Y. Shao, Removal of Cd(II) and Ni(II) from aqueous solutions using activated carbon developed from powder-hydrolyzed-feathers and *Trapa natans* husks, Colloids Surf., A, 560 (2019) 426–433.

[5] J. Štefelová, T. Zelenka, V. Slovák, Biosorption (removing) of Cd(II), Cu(II) and methylene blue using biochar produced by different pyrolysis conditions of beech and spruce sawdust, Wood Sci. Technol., 51 (2017) 1321–1338.

[6] A. Muhmood, J. Lu, R. Kadam, R. Dong, J. Guo, S. Wu, Biochar seeding promotes struvite formation, but accelerates heavy metal accumulation, Sci. Total Environ., 652 (2019) 623–632.

[7] A. Ngigi, Y.S. Ok, S. Thiele-Bruhn, Biochar-mediated sorption of antibiotics in pig manure, J. Hazard. Mater., 364 (2019) 663–670.

[8] S.-Y. Oh, Y.-D. Seo, K.-S. Ryu, Reductive removal of 2,4-dinitrotoluene and 2,4-dichlorophenol with zero-valent iron-included biochar, Bioresour. Technol., 216 (2016) 1014–1021.

[9] C. Fan, C. Guo, Y. Zeng, Z. Tu, Y. Ji, J.R. Reinfelder, M. Chen, W. Huang, G. Lu, X. Yi, The behavior of chromium and arsenic associated with redox transformation of schwertmannite in AMD environment, Chemosphere, 222 (2019) 945–953.

[10] J. Zhu, M. Gan, D. Zhang, Y. Hu, L. Chai, The nature of Schwertmannite and jarosite mediated by two strains of *Acidithiobacillus ferrooxidans* with different ferrous oxidation ability, Mater. Sci. Eng., C, 33 (2013) 2679–2685.

[11] J.M. Bigham, U. Schwertmann, S.J. Traina, R.L. Winland, M. Wolf, Schwertmannite and the chemical modeling of iron in acid sulfate waters, Geochim. Cosmochim. Acta, 60 (1996) 2111–2121.

[12] S. Regenspurg, A. Brand, S. Peiffer, Formation and stability of schwertmannite in acidic mining lakes, Geochim. Cosmochim. Acta, 68 (2004) 1185–1197.

[13] X. Meng, C. Zhang, J. Zhuang, G. Zheng, L. Zhou, Assessment of schwertmannite, jarosite and goethite as adsorbents for efficient adsorption of phenanthrene in water and the regeneration of spent adsorbents by heterogeneous Fenton-like reaction, Chemosphere, 244 (2020) 125523, doi: 10.1016/j.chemosphere.2019.125523.

[14] K. Rout, M. Mohapatra, S. Anand, 2-Line ferrihydrite: synthesis, characterization and its adsorption behaviour for removal of Pb(II), Cd(II), Cu(II) and Zn(II) from aqueous solutions, Dalton Trans., 41 (2012) 3302–3312.

[15] Y. Mamindy-Pajany, C. Hurel, N. Marmier, M. Roméo, Arsenic adsorption onto hematite and goethite, C.R. Chim., 12 (2009) 876–881.

[16] L.-Y. Gao, J.-H. Deng, G.-F. Huang, K. Li, K.-Z. Cai, Y. Liu, F. Huang, Relative distribution of $Cd^{2+}$ adsorption mechanisms on biochars derived from rice straw and sewage sludge, Bioresour. Technol., 272 (2019) 114–122.

[17] M.F. Hamza, Y. Wei, H. Mira, A.-H. Adel, E. Guibal, Synthesis and adsorption characteristics of grafted hydrazinyl amine magnetite-chitosan for Ni(II) and Pb(II) recovery, Chem. Eng. J., 362 (2019) 310–324.

[18] J. Jönsson, P. Persson, S. Sjöberg, L. Lövgren, Schwertmannite precipitated from acid mine drainage: phase transformation, sulphate release and surface properties, Appl. Geochem., 20 (2005) 179–191.

[19] M. Loan, W. Richmond, G. Parkinson, On the crystal growth of nanoscale schwertmannite, J. Cryst. Growth, 275 (2005) e1875–e1881.

[20] Y. Feng, Q. Liu, Y. Yu, Q. Kong, L.-l. Zhou, Y.-d. Du, X.-f. Wang, Norfloxacin removal from aqueous solution using biochar derived from *luffa* sponge, J. Water Supply Res. Technol. AQUA, 67 (2018) 703–714.

[21] S. Tresintsi, K. Simeonidis, G. Vourlias, G. Stavropoulos, M. Mitrakas, Kilogram-scale synthesis of iron oxy-hydroxides with improved arsenic removal capacity: study of Fe(II) oxidation—precipitation parameters, Water Res., 46 (2012) 5255–5267.

[22] L. Albanese, S. Baronti, F. Liguori, F. Meneguzzo, P. Barbaro, F.P. Vaccari, Hydrodynamic cavitation as an energy efficient process to increase biochar surface area and porosity: a case study, J. Cleaner Prod., 210 (2019) 159–169.

[23] M. Mansouri, M. Nademi, M. Ebrahim Olya, H. Lotfi, Study of methyl tert-butyl ether (MTBE) photocatalytic degradation with UV/$TiO_2$-ZnO-CuO nanoparticles, J. Chem. Health Risks, 7 (2017) 19–32.

[24] G. Marbán, BET adsorption reaction model based on the pseudo steady-state hypothesis for describing the kinetics of adsorption in liquid phase, J. Colloid Interface Sci., 467 (2016) 170–179.

[25] G. Meng, A. Li, W. Yang, F. Liu, X. Yang, Q. Zhang, Mechanism of oxidative reaction in the post crosslinking of hyper-crosslinked polymers, Eur. Polym. J., 43 (2007) 2732–2737.

[26] M.K. Aroua, S. Leong, L. Teo, C.Y. Yin, W.M.A.W. Daud, Real-time determination of kinetics of adsorption of lead(II) onto palm shell-based activated carbon using ion selective electrode, Bioresour. Technol., 99 (2008) 5786–5792.

[27] P. Chingombe, B. Saha, R. Wakeman, Sorption of atrazine on conventional and surface modified activated carbons, J. Colloid Interface Sci., 302 (2006) 408–416.

[28] A.W. Marczewski, Analysis of kinetic Langmuir model. Part I: integrated kinetic Langmuir equation (IKL): a new complete analytical solution of the Langmuir rate equation, Langmuir, 26 (2010) 15229–15238.

[29] H. Qiu, M.G. Vijver, E. He, W.J. Peijnenburg, Predicting copper toxicity to different earthworm species using a multicomponent Freundlich model, Environ. Sci. Technol., 47 (2013) 4796–4803.

[30] X.Q. Meng, C.M. Zhang, J. Zhuang, G.Y. Zheng, L.X. Zhou, Assessment of schwertmannite, jarosite and goethite as adsorbents for efficient adsorption of phenanthrene in water and the regeneration of spent adsorbents by heterogeneous Fenton-like reaction, Chemosphere, 244 (2020) 125523, doi: 10.1016/j.chemosphere.2019.125523.

[31] J. Yu, J. Zhang, S. Song, H. Liu, Z. Guo, C. Zhang, Removal of Ni(II) from aqueous solutions using activated carbon with manganese formate hydrate in-situ modification, Colloids Surf., A, 560 (2019) 84–91.

[32] Y. Kang, Z. Guo, J. Zhang, H. Xie, H. Liu, C. Zhang, Enhancement of Ni(II) removal by urea-modified activated carbon derived from *Pennisetum alopecuroides* with phosphoric acid activation, J. Taiwan Inst. Chem. Eng., 60 (2016) 335–341.

[33] Y. Liu, S.P. Sohi, S. Liu, J. Guan, J. Zhou, J. Chen, Adsorption and reductive degradation of Cr(VI) and TCE by a simply synthesized zero valent iron magnetic biochar, J. Environ. Manage., 235 (2019) 276–281.

[34] M. Li, H. Liu, T. Chen, C. Dong, Y. Sun, Synthesis of magnetic biochar composites for enhanced uranium(VI) adsorption, Sci. Total Environ., 651 (2019) 1020–1028.